PHYSICAL REVIEW E, VOLUME 64, 025401(R)

Effects of nonionizing prepulses in high-intensity laser-solid interactions

K. B. Wharton, C. D. Boley, A. M. Komashko, A. M. Rubenchik, J. Zweiback, J. Crane, G. Hays, T. E. Cowan, and T. Ditmire

Lawrence Livermore National Laboratory, University of California, P.O. Box 808, Livermore, California 94550

(Received 4 December 2000; published 17 July 2001)

We present theoretical and experimental evidence that nonionizing prepulses with intensities as low as 10^8-10^9 W/cm^2 can substantially alter high intensity laser-solid interactions. We show that prepulse-heating and vaporization of the target can lead to a preformed plasma once the vapor is ionized by the rising edge of the high-intensity pulse. Our results indicate that peak prepulse intensity is not the only important parameter to consider in determining preformed plasma thresholds, and that a more comprehensive analysis of the prepulse duration and the target material is required.

DOI: 10.1103/PhysRevE.64.025401 PACS number(s): 52.38.Mf, 52.25.Os

The physics of high-intensity laser interactions with solid targets is of wide interest, as near-solid-density plasmas have parameters relevant to inertial confinement fusion as well as being sources of short-pulse x rays [1,2]. At laser intensities above 10^{15} W/cm^2, collisionless processes such as resonance absorption [3] and vacuum heating [4] begin to dominate the laser absorption mechanisms. Both of these mechanisms are highly sensitive to the electron density scale length $L=[(1/n_e)(dn_e/dx)]^{-1}$ at the interaction surface, and therefore a prepulse can strongly affect the primary interaction if it creates a preformed plasma. Often the plasma scale length has been experimentally varied with a short-duration, intentional prepulse [2,5,6].

Apart from intentional prepulses, short-pulse lasers are often superimposed on a longer duration, lower-intensity pedestal of amplified spontaneous emission (ASE). This ASE prepulse has also been observed to affect the interaction of the main laser pulse [7–11], and in some recent ultrahigh intensity experiments it is assumed that the ASE produces a substantial preformed plasma in front of the solid target [12–14]. However, the conditions where ASE becomes relevant have not been well investigated. Preplasma formation threshold intensities quoted in recent literature, on the order of 10^{11} W/cm^2 [15], arise from the assumption that ASE cannot affect the main interaction unless the field intensity is sufficient to cause plasma breakdown on the solid target. Earlier work has shown that ASE in the 10^9 W/cm^2 range affects reflection [8], transmission [9], and x-ray yield [10], although the latter result used uv laser radiation where single-photon ionization effects were present. Laser-solid interactions below both the field- and single-photon-ionization thresholds are well documented in the fields of material processing and analytical chemistry [16–18].

In this Rapid Communication we show that peak ASE intensity is not the only appropriate parameter, and a more comprehensive analysis of the prepulse duration and the target material is required to understand the effect of the ASE. High-intensity experiments are presented to support this conclusion, and puzzling results from some previous experiments are reexamined.

For a nonionizing ASE prepulse incident upon a solid target, the primary effect is the thermal heating of the surface. If the surface reaches temperatures on the order of the boiling point, significant densities of neutral vapor can be outgassed. Although this vapor is not yet ionized, the rising edge of the subsequent high intensity pulse will quickly ionize the atoms, turning a preformed vapor into a preformed plasma. Therefore, the vapor profile is directly related to the electron density profile that will in turn affect resonance absorption (and other absorption mechanisms) of the primary laser pulse.

In this context, prepulse intensity and laser ''contrast'' (the intensity ratio between the ASE and main pulse) are not the most appropriate parameters for ascertaining the preplasma formation. Instead, a more appropriate parameter is an estimate of the energy density at the surface of the target at the time of the main pulse arrival (U_{surf}):

$$U_{\mathrm{surf}}=\frac{\eta I_{\mathrm{avg}}\sqrt{\tau}}{\sqrt{\alpha}} \quad (\text{for } d>\sqrt{2\alpha\tau}), \tag{1a}$$

$$U_{\mathrm{surf}}=\frac{\eta I_{\mathrm{avg}}\tau}{d} \quad (\text{for } d\ll\sqrt{2\alpha\tau}). \tag{1b}$$

Here η is the low-intensity surface absorptivity of the target material, τ is the duration of the ASE, I_{avg} is the average ASE intensity, α is the thermal diffusivity of the target, and d is the target thickness. For targets thicker than the thermal diffusion depth, the first equation applies; for very thin targets one can assume that the heat is deposited evenly. Although Eq. (1) makes the poor assumption that η and α are not functions of temperature, as well as neglecting energy lost to the vapor, U_{surf} yields a more relevant measure of ASE than the usual ''contrast'' ratio (or I_{avg}). The main predictive feature of Eq. (1) is that similar ASE intensities should have very different effects for target materials with different absorptive and thermal properties.

We experimentally explored the effect of ASE on high-intensity interactions using a 35 fs, $\leqslant$130 mJ Ti:sapphire laser (wavelength=820 nm), defocused to a 500 μm spot (full diameter). All shots used *p*-polarization and a 45° angle of incidence. The targets used were 25 μm Ti foils, some overcoated with thin layers of vapor-deposited Al or CH. In order to measure the hot electrons generated at the plasma surface, the primary diagnostic was a time-integrated mea-

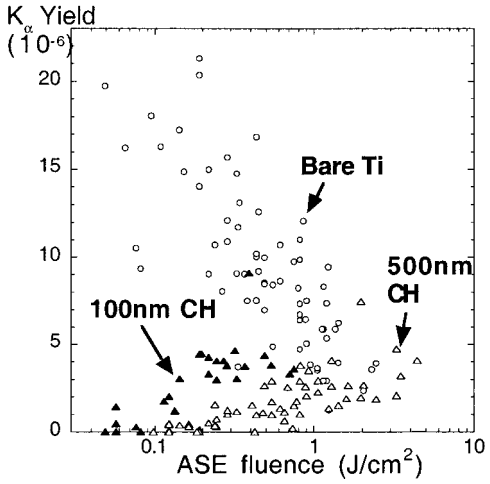

FIG. 1. Conversion efficiency from incident laser energy into outgoing Ti K_α x-ray energy is plotted against the total fluence in the prepulse of the laser. Results are shown for 25-μm-thick bare Ti foil targets (circles), as well as the same targets overcoated with 100 nm CH (closed triangles) and 500 nm CH (open triangles).

sure of the Ti K_α x rays produced by the electrons, observed 22 cm behind the target with a backside illuminated x ray charge-coupled-device camera. The camera was filtered to operate in a single-photon counting regime so that background x rays could be distinguished from the spectral peak [14]. This technique is ''blind'' to any low energy electrons produced by the laser, as only electrons over 5 keV can produce a 4.5 keV Ti K_α photon. The duration and intensity profile of the ASE were measured on every shot with a 200 ps rise-time fast photodiode; a typical ASE profile rose linearly in time until the arrival of the main pulse.

The ASE level preceding the main pulse was varied in three ways. First, the regenerative amplifier of the laser was pumped below saturation so that shot-to-shot variations shifted the ASE intensity between roughly 10^{-6} and 10^{-7} of the peak laser intensity. The duration of the ASE was also systematically varied between 0.5 and 2.0 ns by changing the timing of a fast-slicing Pockels cell in the laser chain. Finally, the total laser energy was varied, always keeping the peak intensity on target between 2×10^{15} and 10^{16} W/cm^2. Because the optimum intensity for Ti K_α production is 4×10^{15} W/cm^2 [19], we do not expect a strong K_α yield variation over this intensity range.

The measured conversion efficiencies from incident laser energy into outgoing Ti K_α x-ray energy (assuming a uniform distribution of x rays into 4π steradians) are plotted in Fig. 1 against total ASE fluence. The results are shown for bare 25-μm-thick Ti foils, as well as 25 μm Ti foils overcoated with a layer of 100 or 500 nm CH. The bare Ti foils show a strong decrease in K_α yield for increasing ASE despite the low absolute ASE levels; the lowest fluence shots on this graph correspond to an average intensity of only 10^8 W/cm^2 over 0.5 ns. This strongly indicates that some process in the nonionizing 10^8-10^9 W/cm^2 range affects the absorption of the high intensity laser. The neutral-vapor hypothesis presented above is supported by the differences between bare-Ti and CH-coated targets in Fig. 1. Unlike the

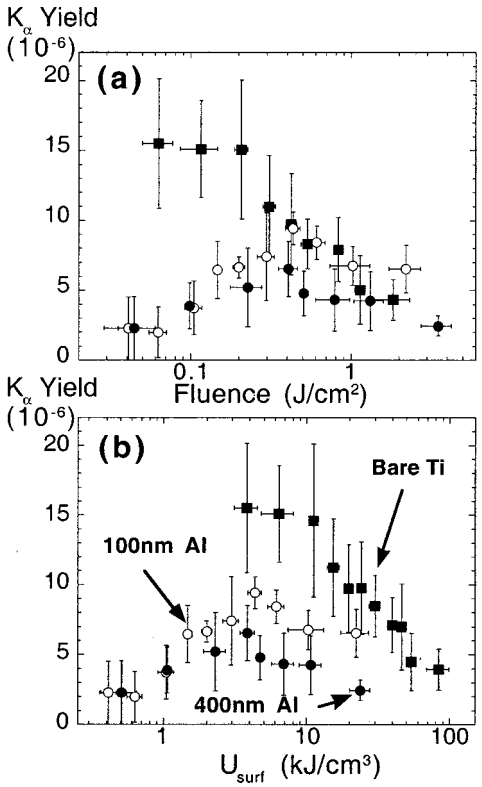

FIG. 2. (a) shows the conversion efficiency from incident laser energy into outgoing Ti K_α x-ray energy plotted against total ASE fluence. Results are shown for 25-μm-thick bare Ti foil targets (squares), as well as the same targets overcoated with 100 nm A (open circles) and 400 nm CH (closed circles). (b) shows the same data plotted against the prepulse parameter $U_{\rm surf}$ as defined in Eq. (1), which scales as the energy density in the surface of the target.

bare targets, the yield from the coated targets increases with larger ASE fluences. This is consistent with the above model; the thin CH layer will be transparent to the low intensity ASE and will limit vapor outgassing from the heated Ti foil. However, at some point the heated Ti can melt back through the CH layer, producing CH vapor for larger ASE levels.

For a comparison of opaque targets, we deposited a layer of Al onto the Ti foils in place of the transparent CH, so that the ASE energy would be absorbed on the surface. Figure 2(a) shows the conversion efficiency into K_α x rays as a function of the ASE fluence. The results are shown for bare 25 μm Ti foils (the same data set as Fig. 1, binned for clarity), as well as 25 μm Ti foils coated with a vapor-deposited layer of 100 or 400 nm Al. These data seem to indicate quite different optimal fluence levels for the different materials: on bare Ti the optimum yield lies near the lowest ASE fluence (0.05 J/cm^2) while the yield from the Al-coated targets peaks at nearly an order of magnitude higher ASE fluence (near 0.4 J/cm^2).

The importance of the deposited surface energy density, however, becomes apparent when these yields are plotted against $U_{\rm surf}$ [as determined from Eq. (1)] in Fig. 2(b). For bare Ti targets $U_{\rm surf}$ is calculated using the low-intensity value for η (40%) and the melting-point value for α (0.07 cm^2/s). The 400 nm Al-coated targets used the corresponding

aluminum parameters of $\eta = 20\%$ and $\alpha = 0.5$ cm^2/s. The 100 nm Al-coated targets were sufficiently thin to apply Eq. (1b), which assumes the absorbed ASE energy was evenly deposited throughout the Al layer (and minimal thermal conduction into the much lower thermal conductivity Ti substrate). In Fig. 2(b) the qualitative scaling is now similar between targets: both Al-coated targets show a peak in the K_α yield at a surface energy density of 4–5 kJ/cm^3, which is also consistent with the available data from the bare Ti targets. This implies that this energy density corresponds to a vapor scale length that optimizes the production of fast electrons.

In order to estimate the density and scale length of this vapor plume, we simulated the heat deposition with a 1D hydrodynamics and vaporization code [20] designed to model material drilling by laser intensities between 10^8 and 10^{11} W/cm^2. This code (THALES) uses temperature-dependent material properties (absorptivity, diffusivity, etc.) and calculates heat transfer in the target, vaporization, and hydrodynamics of the expanding plume. For a given laser intensity profile, the code is believed to provide a good estimate of the target surface temperature. However, the mean free path in the outgassed vapor is on the order of a micron, which is comparable to the vapor scale length. For this reason we analytically computed the vapor density profile from the temperature history of the target, assuming the velocity distribution of the vapor at the surface is a one-directional Maxwellian [21]. From the vapor density, a plasma density is then calculated by noting that the intensity of our main laser pulse would be expected to triply ionize the Al vapor and $4x$-ionize the Ti vapor.

The final plasma density profile from these simulations and calculations are shown in Fig. 3 for both Ti and Al targets and various ASE intensities assuming a 1.0 ns ASE ramp. There is a clear material difference; Ti targets require less of an ASE prepulse than Al targets to produce similar plasma densities. Also, it is apparent that ASE intensities on the order of 10^9 W/cm^2 can easily produce overcritical plasmas via the vaporization mechanism described above. This is typically two orders of magnitude smaller than previous estimates of relevant ASE levels.

For both overdense plasma density profiles shown in Fig. 3, the scale length L is very close to 0.2 μm. This is near to the optimum plasma scale length for resonance absorption for our laser parameters [3]. However, there is a quantitative difference between the $U_{\rm surf} = 12-24$ kJ/cm^3 which yield the optimum plasma profiles and the $U_{\rm surf} = 4-5$ kJ/cm^3 seen to optimize the K_α x-ray yield in our experiments. Indeed, the lower-density profiles shown in Fig. 3 are closer to the latter numbers, but those underdense plasmas would not be expected to enhance resonance absorption. A number of factors could give rise to this quantitative difference, including inaccurate estimates for the liquid state properties used in THALES, which are not well established. Another possibility is that an underdense plasma shelf might optimize the hot electron production not through resonance absorption, but through vacuum heating [4,22]. (We also note that ASE-induced corrugations of the target surface has been proposed as an absorption-altering mechanism [8].) Nonetheless, the

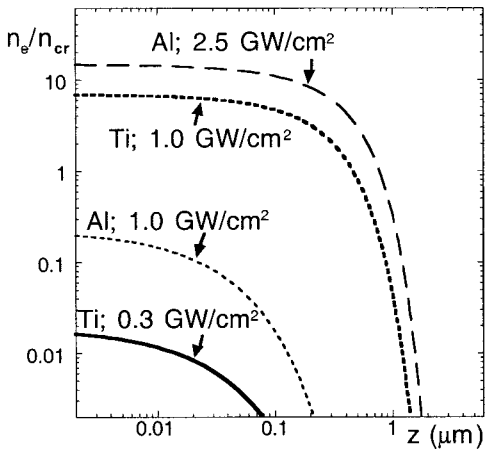

FIG. 3. Calculated plasma density profiles are plotted in units of electron density (normalized to the critical density for 820 nm, $n_{\rm cr} = 1.66\times10^{21}$ cm^{-3}), as a function of distance from the surface of the target. Results are shown for 400 nm Al targets (thin lines) and 25 μm Ti targets (thick lines), for peak ASE intensities of 3×10^8 W/cm^2 (solid line), 10^9 W/cm^9 (short-dashed lines), and 2.5×10^9 W/cm^{-2} (long-dashed line). All ASE profiles are 1 ns in duration, and have a linearly rising profile; i.e., the average intensity is half of the peak intensity. Equivalent values of $U_{\rm surf}$ [from Eq. (1)] are as follows: 4.5 kJ/cm^3 (lower intensity Al), 11.5 kJ/cm^3 (higher intensity Al), 7 kJ/cm^3 (lower intensity Ti), and 24 kJ/cm^3 (higher intensity Ti).

THALES simulation confirms the qualitative material scaling seen in the experiments, and also demonstrates that overcritical plasmas can be generated by target outgassing.

Further evidence for the relevance of these ASE levels can be found in previously published high-intensity laser-solid experiments. Several groups have observed a dramatic difference between high-intensity laser absorption in opaque and transparent targets [11,14,23], which can likely be explained in terms of ASE effects. In particular, Ref. [11] noted that a difference in x-ray yield from Al and glass targets was strongly dependent on the duration of the ASE before the arrival of the main pulse, yet an interferometric diagnostic saw no preformed plasma on either target at standard ASE levels. Neutral vapor outgassing may explain these results; the surface absorption would be much higher in Al than in glass, and therefore the ASE could cause neutral vapor outgassing on only the Al targets. However, a plume of neutral vapor would be invisible to standard interferometric diagnostics before the arrival of the main pulse.

Other results in the literature also support this model. Jiang *et al.* [24] measured the density of x-ray-emitting regions from laser-solid interactions, and found very different results between Ti, Al, and NaCl targets. Although these experiments were performed at intensities of 10^{19} W/cm^2, their stated contrast ratio of 10^{-10}:1 indicates that their ASE was $\sim10^9$ W/cm^2. The authors consider the possibility of a prepulse, but observe that in transparent targets (NaCl) the x-ray emission comes from a solid density plasma, and so they rule out a relevant prepulse which might pre-expand their target. However, the lower plasma density measured in their Al targets (and the lack of signal from Ti targets) hint

that ASE may have been affecting these opaque targets, sparing only the transparent NaCl.

This target vaporization analysis should take into account not only changes in target material, but also thickness variations of thin foil targets [where Eq. 1(b) applies]. Feurer *et al.* [25] report evidence of resistive inhibition of hot electron transport through very thin (400–700 nm) Al layers on a Cu substrate. This is at odds with high levels of hot electrons that have been seen to propagate through much thicker ($\sim$500 μm) layers of Al in other experiments [14]. Another interpretation of these results is that increasing the thickness of the Al layer from 400 to 700 nm allowed the prepulse heat to diffuse into the target, preventing surface vaporization. Note that the thermal diffusion depth for a 3 ns ASE pulse in warm Al is $(2\alpha\tau)^{1/2}=550$ nm. The experiments presented here are not exactly applicable to this previous work, as our substrate (Ti) has a lower thermal conductivity than Cu, so further experiments would be needed to test this interpretation.

With the experiments presented above, we show that ASE-induced target vaporization and subsequent formation of preformed plasmas is an important effect in laser-solid interactions. This conclusion has implications for a wide range of experiments, not only in setting relevant goals for ASE-supression in high power laser systems, but also in target design, data interpretation, and comparison between various high-intensity experiments.

The authors gratefully thank D. Munro and S. Hatchett for crucial contributions as well as R. A. Smith for useful discussions. This work was conducted under the auspices of the U.S. Department of Energy by Lawrence Livermore National Laboratory under Contract No. W-7405-ENG-48.

[1] D. Kühlke, U. Herpes, and D. Von der Linde, Appl. Phys. Lett. **50**, 1785 (1987).
[2] M. M. Murnane, H. C. Kapteyn, and R. W. Falcone, Phys. Rev. Lett. **62**, 155 (1989).
[3] V. L. Ginzburg, *The Propagation of Electromagnetic Waves in Plasmas* (Pergamon, New York, 1964), p. 260.
[4] F. Brunel, Phys. Rev. Lett. **59**, 52 (1987).
[5] H. W. K. Tom and O. R. Wood, Appl. Phys. Lett. **54**, 517 (1989).
[6] S. Bastiani *et al.*, Phys. Rev. E **56**, 7179 (1997); Th. Schlegel *et al., ibid.* **60**, 2209 (1999).
[7] O. Willi *et al.*, Europhys. Lett. **10**, 141 (1989).
[8] J.-C. Gauthier *et al.*, in *Laser Interactions with Atoms, Solids, and Plasmas*, NATO ASI Series, edited by R. M. More (Plenum, New York, 1994), p. 357.
[9] T. R. Boehly *et al.*, Phys. Plasmas **8**, 231 (2001).
[10] J. A. Cobble *et al.*, J. Appl. Phys. **69**, 3369 (1991).
[11] R. Benattar *et al.*, Opt. Commun. **88**, 376 (1992).
[12] U. Teubner *et al.*, Phys. Rev. E **54**, 4167 (1996).
[13] F. N. Beg *et al.*, Phys. Plasmas **4**, 447 (1997).
[14] K. B. Wharton *et al.*, Phys. Rev. Lett. **81**, 822 (1998).
[15] B. F. K. Young, B. G. Wilson, D. F. Price, and R. E. Stewart, Phys. Rev. E **58**, 4929 (1998).
[16] Yu. V. Afanasyev, O. N. Krokhin, and G. V. Sklizkov, IEEE J. Quantum Electron. **QE-2**, 483 (1966).
[17] V. A. Batanov, F. V. Bunkin, A. M. Prokhorov, and V. B. Fedorov, Sov. Phys. JETP **36**, 311 (1973).
[18] B. N. Chichov *et al.*, Appl. Phys. A: Mater. Sci. Process. **63**, 109 (1996).
[19] Ch. Reich, P. Gibbon, I. Uschmann, and E. Förster, Phys. Rev. Lett. **84**, 4846 (2000).
[20] C. D. Boley and J. T. Early, Proceedings of the International Congress on Applications of Lasers and Electro-Optics (ICALEO) (Laser Institute of America, Orlando, FL, 1994), Vol. 2500, p. 499.
[21] S. I. Anisimov *et al.*, *Effects of High-Power Radiation on Metals* (NTIS, Springfield, VA, 1971).
[22] P. Gibbon and A. R. Bell, Phys. Rev. Lett. **68**, 1535 (1992).
[23] A. Saemann and K. Eidmann, Appl. Phys. Lett. **73**, 1334 (1998).
[24] Z. Jiang *et al.*, Phys. Plasmas **2**, 1702 (1995).
[25] T. Feurer *et al.*, Phys. Rev. E **56**, 4608 (1997).